

# GAN-based Data Augmentation for Chest X-ray Classification

Shobhita Sundaram\*

Neha Hulkund\*

shobhita@mit.edu

nhulkund@mit.edu

Massachusetts Institute of Technology  
Cambridge, Massachusetts, USA

## Abstract

A common problem in computer vision – particularly in medical applications – is a lack of sufficiently diverse, large sets of training data. These datasets often suffer from severe class imbalance. As a result, networks often overfit and are unable to generalize to novel examples. Generative Adversarial Networks (GANs) offer a novel method of synthetic data augmentation. In this work, we evaluate the use of GAN-based data augmentation to artificially expand the CheXpert dataset of chest radiographs. We compare performance to traditional augmentation and find that GAN-based augmentation leads to higher downstream performance for underrepresented classes. Furthermore, we see that this result is pronounced in low data regimens. This suggests that GAN-based augmentation is a promising area of research to improve network performance when data collection is prohibitively expensive.

## CCS Concepts

• **Computing methodologies** → **Neural networks**; • **Applied Computing** → *Health informatics*.

## ACM Reference Format:

Shobhita Sundaram and Neha Hulkund. 2021. GAN-based Data Augmentation for Chest X-ray Classification. In *Proceedings of KDD DSHealth '21*. ACM, New York, NY, USA, 5 pages. <https://doi.org/10.1145/1122445.1122456>

## 1 Introduction

Convolutional Neural Networks (CNNs) have demonstrated tremendous success in recent years for visual tasks such as object recognition and segmentation. The application of such networks to clinical tasks – including the segmentation of organs/pathologies [10], and classification of medical images [23] [1]– promises to augment medical decision-making.

However, large amounts of labeled data are required to train high-performing CNNs. A lack of sufficiently large, diverse sets of training data typically results in models that overfit on the training data [17] and generalize poorly [22]. Labelling medical imaging data is both expensive and time-consuming; lack of sufficiently diverse labelled training data is one of the major barriers to developing models fit for clinical use. Furthermore, medical data often suffers from the problem of class imbalance [8], where samples of one

pathology may be far more prevalent than others, leading to biased models [9].

In this work, we investigate whether incorporating data generated by Generative Adversarial Networks (GANs) into training data as a data augmentation technique can improve the efficacy of Deep Neural Networks in diagnosing lung diseases from chest radiographs. While GAN augmentation requires an additional trained network – as opposed to standard augmentation techniques – our work demonstrates that this technique leads to performance improvements, which are particularly important in high stakes clinical decision-making.

While several prior works have tested the efficacy of GAN-based data augmentation, there are limited studies that compare effectiveness of GAN augmentation with more traditional methods of fixing class imbalance [18]. We aim to bridge this gap by exploring the problem of class imbalance across different data regimens, comparing the performance of traditional and GAN data augmentation methods.

The contributions of this paper are:

- We demonstrate the efficacy of GAN-based data augmentation compared to standard data augmentation and no augmentation techniques in correcting class imbalances that are found in the Stanford CheXpert dataset.
- We show that GAN data augmentation is most effective when used with small, significantly imbalanced datasets, and has limited impact for large datasets.

## 2 Related Work

GAN data augmentation has been found useful for diversifying datasets by producing novel samples [5] [20]. Sanfort et al. and Rashid et al. found that using CycleGAN for augmentation in segmentation and classification tasks improved performance significantly, demonstrating the potential of GAN-based data augmentation for medical applications [19][16].

GAN data augmentation has been used to correct class imbalance with moderate success on imbalanced MNIST and CIFAR datasets using balancing GANs (BAGANs) [11], as well as brain tumor datasets [14]. Further works have found that synthetic data augmentation for class imbalance is more effective for low data regimens, where the model suffers most from overfitting and lack of generalization [2]. As far as we know this finding has not been studied in medical datasets, nor systematically compared to standard augmentation techniques.

## 3 CheXpert Dataset

Our experiment uses CheXpert, a publicly available dataset from Stanford Hospital of 224,316 frontal and lateral chest radiographs of 65,240 patients [7]. Each radiograph is labeled with a 14-element vector, where each element indicates the label for a particular pathology in the image; 1 corresponds to positive, 0 to negative, and -1

\*Both authors contributed equally to this research.

Permission to make digital or hard copies of all or part of this work for personal or classroom use is granted without fee provided that copies are not made or distributed for profit or commercial advantage and that copies bear this notice and the full citation on the first page. Copyrights for components of this work owned by others than ACM must be honored. Abstracting with credit is permitted. To copy otherwise, or republish, to post on servers or to redistribute to lists, requires prior specific permission and/or a fee. Request permissions from [permissions@acm.org](mailto:permissions@acm.org).

*Proceedings of KDD DSHealth, August 14–18, 2021,*

© 2021 Association for Computing Machinery.

ACM ISBN 978-1-4503-XXXX-X/18/06...\$15.00

<https://doi.org/10.1145/1122445.1122456>

Pathology	Positive (%)	Uncertain (%)	Negative (%)
No Finding	16627 (8.86)	0 (0.0)	171014 (91.14)
Enlarged Cardiom.	9020 (4.81)	10148 (5.41)	168473 (89.78)
Cardiomegaly	23002 (12.26)	6597 (3.52)	158042 (84.23)
Lung Lesion	6856 (3.65)	1071 (0.57)	179714 (95.78)
Lung Opacity	92669 (49.39)	4341 (2.31)	90631 (48.3)
Edema	48905 (26.06)	11571 (6.17)	127165 (67.77)
Consolidation	12730 (6.78)	23976 (12.78)	150935 (80.44)
Pneumonia	4576 (2.44)	15658 (8.34)	167407 (89.22)
Atelectasis	29333 (15.63)	29377 (15.66)	128931 (68.71)
Pneumothorax	17313 (9.23)	2663 (1.42)	167665 (89.35)
Pleural Effusion	75696 (40.34)	9419 (5.02)	102526 (54.64)
Pleural Other	2441 (1.3)	1771 (0.94)	183429 (97.76)
Fracture	7270 (3.87)	484 (0.26)	179887 (95.87)
Support Devices	105831 (56.4)	898 (0.48)	80912 (43.12)

Figure 1: Pathologies Present in Dataset [7]

Dataset Size	Lung Le- sion	Pleural Other	Fracture	Augmented Dataset
2050 (1%)	500	550	500	3600
20371 (10%)	3500	4000	3500	49829
100850 (50%)	15000	17000	15000	147850
201391 (100%)	30000	35000	30000	296391

Table 1: Number of generated images for each underrepresented class across different data regimens for GAN-augmentation

to uncertain. The different pathologies and their proportions in the dataset are detailed in Fig. 1.

We employ a label-smoothing technique of mapping the uncertainty labels to 1, previously shown by Pham et al to improve performance in the dataset [12]. Further preprocessing includes resizing the images to 224 by 224 pixels, performing a center crop for uneven aspect ratios, and scaling pixel values to  $[-1024, 1024]$  [3].

As shown in Fig. 1, the CheXpert data suffers from significant class imbalance. We perform data augmentation on three pathologies which each make up less than 5% of the dataset: Lung Lesion, Pleural Other, and Fracture.

To examine the augmentation efficacy over different sizes of datasets, we perform all experiments over the following subsets of the dataset: 1%, 10%, 50%, and 100%, further detailed in Section 5.1.

## 4 Approach

Our approach consists of generating GAN images in which at least one of the 3 underrepresented pathologies are present. These GAN-generated images are then integrated with the original CheXpert data subset, such that the class imbalance is reduced. The process is shown in Fig 3. We evaluate the relative efficacy of training on GAN-augmented data by comparing to separate models trained with standard data augmentation and no data augmentation.

### 4.1 Classification model

In previous works, the DenseNet-121 architecture has achieved a high performance on chest X-ray classification, as demonstrated in Rajpurkar et al and Pham et al [15] [13]. We transfer train TorchXRyVision’s DenseNet-121, pretrained on ImageNet, for all experiments [3]. For each data augmentation procedure (refer to

4.2), we train using  $\{1\%, 10\%, 50\%, 100\%\}$  subsets of the full CheXpert dataset.

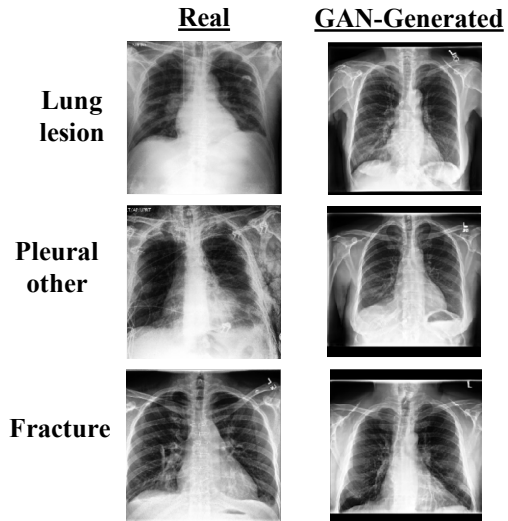


Figure 2: Sample synthetic chest X-rays generated by a pre-trained GAN for underrepresented classes in CheXpert

### 4.2 Data augmentation frameworks

**GAN-based augmentation** Our proposed data augmentation framework employs GANs to generate synthetic images of underrepresented pathologies, thus correcting for class imbalance in the training dataset.

We use a Conditional GAN with mirrored structures for the generator and discriminator, that was progressively pretrained on chest X-rays from the CheXpert dataset as described in [6]. The trained GAN generates radiographs that are difficult to distinguish from real images [6]. The Conditional GAN takes as input a length-14 label vector  $\{x_1, x_2, \dots, x_{14}\}$ , where  $x_i = 1$  if pathology  $i$  is present, and  $x_i = 0$  otherwise (note that if  $x_0 = 1$  then the classification is "No Finding"). As output, it generates a chest X-ray with the corresponding pathologies present. Note that this gives us precise control over the exact label vector for each generated image.

Given an underrepresented pathology  $p$ ,  $L_p$  is the subset of label vectors in the real dataset in which  $p$  is present (i.e. all label vectors for which  $x_p = 1$ ). We uniformly sample with replacement from  $L_p$ . Each sampled label vector is inputted to the GAN to generate a synthetic chest X-ray in which  $p$  is present. Note that a synthetic image with  $p$  present may contain other pathologies as well, to preserve any co-occurring relationships between pathologies that may be important towards classification. We then combine the set of generated images with the original image dataset to produce the more balanced augmented dataset. Sample synthetic images are presented alongside real X-rays in Fig. 2

For each of the underrepresented pathologies (lung lesion, pleural other, fracture) we generate the minimum number of synthetic images such that each pathology is represented in at least 15% of the combined augmented dataset. We choose the 15% threshold because the majority of CheXpert pathologies are present in 5 – 26% of images; thus 15% representation enables a more balanced dataset.

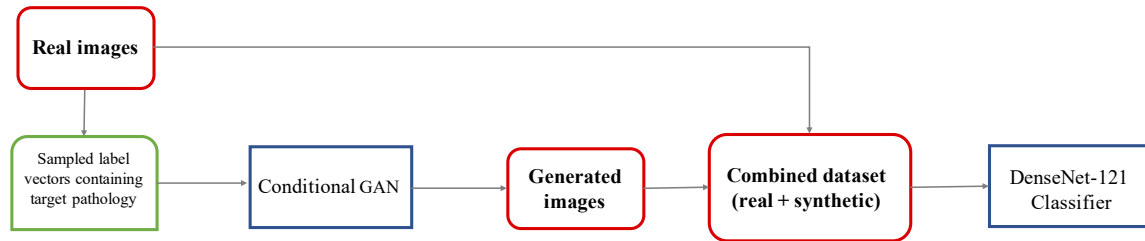


Figure 3: Illustration of the proposed GAN-based data augmentation method. Our method combines GAN-generated images with real images of underrepresented pathologies to produce an augmented dataset that can be used for training.

Dataset Size	Pathology	No Augmentation	Standard Augmentation	GAN Augmentation
1%	Lung Lesion	0.727	0.728	0.758
	Pleural Other	0.566	0.550	0.594
	Fracture	0.583	0.601	0.656
10%	Lung Lesion	0.790	0.796	0.803
	Pleural Other	0.632	0.655	0.670
	Fracture	0.700	0.723	0.742
50%	Lung Lesion	0.826	0.822	0.828
	Pleural Other	0.710	0.696	0.706
	Fracture	0.789	0.780	0.793
100%	Lung Lesion	0.835	0.832	0.834
	Pleural Other	0.721	0.712	0.727
	Fracture	0.811	0.793	0.807

Table 2: AUC performance across augmentation techniques and dataset regimens for augmented classes

The exact number of images generated for each training data subset is shown in Table 1.

**Standard data augmentation** As a benchmark comparison to no augmentation and GAN augmentation, we apply standard data augmentation techniques of randomly vertical/horizontal flipping a subset of the X-rays. We use these transformations because they have been shown to lead to performance gains for the chest X-ray datasets in previous works [21]. In each epoch of the training process, we apply these transforms on-the-fly with probability 0.5 to each image in the batch.

**No data augmentation** We additionally train DenseNet-121 without any augmentations. Training and evaluating this network creates a baseline with which to compare the networks trained on GAN-augmented data and standard-augmented data.

## 5 Results

### 5.1 Experimental setup

We train DenseNet-121 for a 14-way classification task, where each input image may have multiple pathologies represented. We conduct 3 main experiments (GAN-based augmentation, standard augmentation, no augmentation), and for each experiment we train using randomly sampled {1%, 10%, 50%, 100%} subsets of the training dataset. We use a 90%–5%–5% split for training/validation/testing. The same hold-out test set, consisting of 5% of the original dataset, is used to evaluate all networks, while the random training/validation split takes place at train-time.

All networks are trained using binary cross entropy loss for up to 10 epochs. While training for more epochs may lead to higher

performance, computational constraints limit us to 10 epochs per experiment. For each experiment, we conduct the following hyperparameter search:

- Learning rate: { $1e-2$ ,  $5e-3$ ,  $1e-3$ }
- Batch size: {16, 32, 64}
- Optimizer: {Momentum, Adam}

In the following sections, all AUCs reported are for the networks and hyperparameters that achieve the highest validation AUC.

### 5.2 Model performance

Model performance via ROC-AUC score across the augmentation techniques and dataset regimens is detailed in Table 2. For the smallest data regimen (1%) we see significant gains in performance when training with GAN-augmentation data as opposed to standard or no augmentation. This is evident across all pathologies, with a 0.03 AUC gain between GAN augmentation and no augmentation for lung lesions and pleural other, and a 0.07 AUC gain for fracture. Note that using standard augmentation also improves performance compared to no augmentation, however less so than GAN augmentation. Our results for the second-smallest data regimen (10%) also demonstrate an improvement with GAN augmentation across the pathologies. These positive results demonstrate that models trained with GAN augmentation outperform those trained with standard or no augmentation in small data regimens.

In the larger data regimens, we see either minimal or negative performance improvement for GAN and standard augmentation techniques as compared to no augmentation. For the data regimen of 100%, both augmentation techniques have a lesser performance than the original dataset for the lung lesion and fracture pathologies.

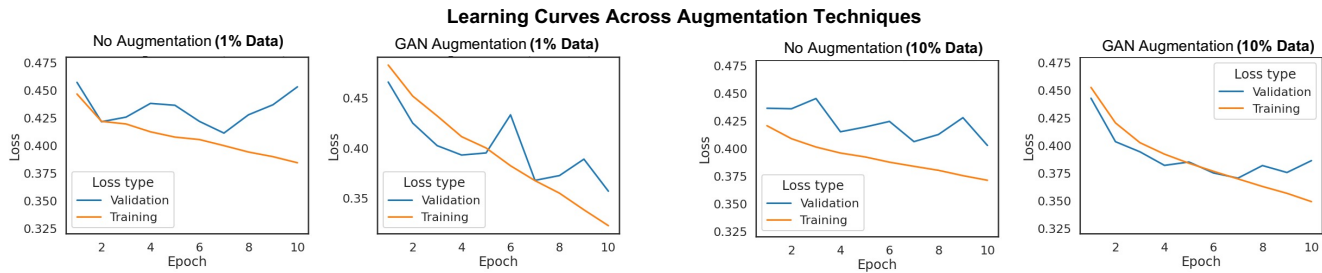


Figure 4: Comparison of training and validation loss curves for no augmentation and GAN-based augmentation training

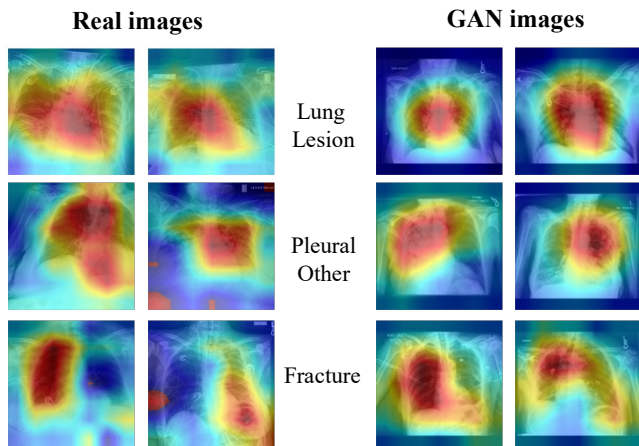


Figure 5: Class Activation Maps (CAMs) produced by a network trained with GAN augmentation, for real images and GAN-generated images.

However, in the pleural other pathology, we see a 0.006 AUC gain from no augmentation to GAN augmentation. Since pleural other is the most imbalanced class of the three, this indicates that even at high data regimens, GAN augmentation can be useful for significant data imbalances.

Additionally, we observe that standard data augmentation has a worse performance than no augmentation across all pathologies in large data regimens. Our standard augmentation method uses flips; thus this result could be attributed to the presence of structures in the radiographs that lack left-right or up-down invariance. Alternate techniques could include blurring or saturation/hue jittering. The performance decrease for standard augmentation could also be alleviated with training standard-augmentation models for more epochs (we were unable to do so due to computational constraints).

### 5.3 Comparison of learning curves

In Figure 4, we compare learning curves when training with no augmentation and GAN augmentation. We find that GAN based augmentation alleviates overfitting in the low-data regimen of 1%. In the final epoch, we see a 0.03 difference between training and validation loss in the GAN augmented model and a 0.06 difference in the non-augmented model. In the 10% regimen, the overfitting between the two models is comparable, with the GAN-augmented and non-augmented loss differences at 0.03 and 0.04, respectively.

This is consistent with our AUC results, indicating that adding synthetic images can alleviate overfitting for very low data regimens, but does not necessarily help as the dataset size increases.

### 5.4 Visualization of class activation maps

We gain further qualitative insight regarding the use of GAN-based augmentation through class activation maps (CAMs) [4]. For a particular category, CAMs indicate the most discriminative image regions used to identify the category by projecting the weights of the output layer onto the final convolutional feature maps.

In Figure 5, we visualize CAMs for the DenseNet trained with GAN-augmentation on 100% of the CheXpert training data, as this model had the highest overall performance. For each of the 3 underrepresented pathologies, we visualize CAMs for real X-rays and GAN-generated X-rays. Note that for each pathology, the resultant heatmaps appear similar between real and GAN-generated images, indicating that the network activations may be similar between the two. The similarity of CAMs provides some evidence that the network has not overfit to real or GAN images, despite being trained on mostly GAN images for the imbalanced classes.

Furthermore, for all CAMs, the highest activations appear localized to a particular region in each X-ray. The emergence of high activation at specific locations means that CAMs may provide useful, interpretable insight in a clinical setting regarding the parts of an X-ray that indicate specific pathologies.

## 6 Conclusion

In this work, we perform a comparison of GAN data-augmented models to standard augmented and non-augmented models across different data regimens. Our findings indicate that GAN-based data augmentation may be an effective tool for correcting class imbalanced medical datasets. We demonstrate AUC performance gains as compared to standard and no augmentation techniques across dataset sizes and pathologies. Additionally, we find that GAN-data augmented models overfit less in low-data regimens. From our results, we conclude that augmentation techniques are particularly effective across low-data regimens and show promise for correcting class imbalance in medical applications, where datasets are often both small and skewed. Note that this study assumes access to a GAN that has been pretrained on a large data set, which may not always be the case in a clinical setting. Future work may investigate whether the advantages of GAN-based augmentation also exist when using GANs trained on smaller datasets.

## References

[1] Martin G Ting DSW Karthikesalingam A King D Ashrafian H Darzi A. Aggarwal R, Sounderajah V. 2021. Diagnostic accuracy of deep learning in medical imaging: a systematic review and meta-analysis. *NPJ Digit Med* 4 (2021).

- [2] Anthreas Antoniou, Amos Storkey, and Harrison Edwards. 2018. Data Augmentation Generative Adversarial Networks. <https://openreview.net/forum?id=S1AuvWRZ>
- [3] Joseph Paul Cohen, Mohammad Hashir, Rupert Brooks, and Hadrien Bertrand. 2020. On the limits of cross-domain generalization in automated X-ray prediction. In *Medical Imaging with Deep Learning*. <https://arxiv.org/abs/2002.02497>
- [4] D. Erhan, Yoshua Bengio, Aaron C. Courville, and Pascal Vincent. 2009. Visualizing Higher-Layer Features of a Deep Network.
- [5] I. Goodfellow, Jean Pouget-Abadie, Mehdi Mirza, B. Xu, David Warde-Farley, S. Ozair, Aaron C. Courville, and Yoshua Bengio. 2014. Generative Adversarial Networks. *ArXiv abs/1406.2661* (2014).
- [6] Tianyu Han, Sven Nebelung, Christoph Haarbuerger, Nicolas Horst, Sebastian Reinartz, Dorit Merhof, Fabian Kiessling, Volkmar Schulz, and Daniel Truhn. 2019. Breaking Medical Data Sharing Boundaries by Employing Artificial Radiographs. *bioRxiv* (2019). <https://doi.org/10.1101/841619> arXiv:<https://www.biorxiv.org/content/early/2019/11/14/841619.full.pdf>
- [7] Jeremy A. Irvin, Pranav Rajpurkar, M. Ko, Yifan Yu, Silvana Ciurea-Ilcus, Chris Chute, H. Marklund, Behzad Haghgoo, Robyn L. Ball, K. Shpanskaya, J. Seekins, D. Mong, S. Halabi, J. Sandberg, R. Jones, D. Larson, C. Langlotz, B. Patel, M. Lungren, and A. Ng. 2019. CheXpert: A Large Chest Radiograph Dataset with Uncertainty Labels and Expert Comparison. In *AAAI*.
- [8] Nathalie Japkowicz and Shaju Stephen. 2002. The class imbalance problem: A systematic study. *Intelligent data analysis* 6, 5 (2002), 429–449.
- [9] Bartosz Krawczyk. 2016. Learning from imbalanced data: open challenges and future directions. *Progress in Artificial Intelligence* 5, 4 (2016), 221–232.
- [10] Xiangbin Liu, Liping Song, Shuai Liu, and Yudong Zhang. 2021. A Review of Deep-Learning-Based Medical Image Segmentation Methods. *Sustainability* 13, 3 (2021). <https://doi.org/10.3390/su13031224>
- [11] G. Mariani, F. Scheidegger, R. Istrate, C. Bekas, and A. Malossi. 2018. BAGAN: Data Augmentation with Balancing GAN. *ArXiv abs/1803.09655* (2018).
- [12] Hieu H. Pham, Tung T. Le, D. Ngo, Dat Q. Tran, and H. Q. Nguyen. 2021. Interpreting Chest X-rays via CNNs that Exploit Hierarchical Disease Dependencies and Uncertainty Labels. *Neurocomputing* 437 (2021), 186–194.
- [13] Hieu H. Pham, Tung T. Le, Dat Q. Tran, D. Ngo, and H. Q. Nguyen. 2019. Interpreting chest X-rays via CNNs that exploit disease dependencies and uncertainty labels. *ArXiv abs/1911.06475* (2019).
- [14] A. B. Qasim, Ivan Ezhov, S. Shit, Oliver Schoppe, Johannes C. Paetzold, A. Sekuboyina, Florian Kofler, Jana Lipková, Hongwei Li, and B. Menze. 2020. Red-GAN: Attacking class imbalance via conditioned generation. Yet another medical imaging perspective. *ArXiv abs/2004.10734* (2020).
- [15] Pranav Rajpurkar, Jeremy A. Irvin, Robyn L. Ball, Kaylie Zhu, B. Yang, Hershel Mehta, T. Duan, D. Ding, Aarti Bagul, C. Langlotz, B. Patel, K. Yeom, K. Shpanskaya, F. Blankenberg, J. Seekins, T. Amrhein, D. Mong, S. Halabi, Evan Zucker, A. Ng, and M. Lungren. 2018. Deep learning for chest radiograph diagnosis: A retrospective comparison of the CheXNeXt algorithm to practicing radiologists. *PLoS Medicine* 15 (2018).
- [16] Haroon Rashid, M. Tanveer, and H. Khan. 2019. Skin Lesion Classification Using GAN based Data Augmentation. *2019 41st Annual International Conference of the IEEE Engineering in Medicine and Biology Society (EMBC)* (2019), 916–919.
- [17] Leslie Rice, Eric Wong, and Zico Kolter. 2020. Overfitting in adversarially robust deep learning. In *Proceedings of the 37th International Conference on Machine Learning (Proceedings of Machine Learning Research, Vol. 119)*, Hal Daumé III and Aarti Singh (Eds.). PMLR, 8093–8104. <http://proceedings.mlr.press/v119/rice20a.html>
- [18] Vignesh Sampath, I. Mautua, Juan José Aguilar Martín, and Aitor Gutierrez. 2020. A Survey on Generative Adversarial Networks for imbalance problems in computer vision tasks.
- [19] V. Sandfort, Ke Yan, P. Pickhardt, and R. Summers. 2019. Data augmentation using generative adversarial networks (CycleGAN) to improve generalizability in CT segmentation tasks. *Scientific Reports* 9 (2019).
- [20] Connor Shorten and T. Khoshgoftaar. 2019. A survey on Image Data Augmentation for Deep Learning. *Journal of Big Data* 6 (2019), 1–48.
- [21] O. Stephen, M. Sain, U. J. Maduh, and Do-Un Jeong. 2019. An Efficient Deep Learning Approach to Pneumonia Classification in Healthcare. *Journal of Healthcare Engineering* 2019 (2019).
- [22] David Stutz, Matthias Hein, and Bernt Schiele. 2019. Disentangling adversarial robustness and generalization. In *Proceedings of the IEEE/CVF Conference on Computer Vision and Pattern Recognition*. 6976–6987.
- [23] S. Kevin Zhou, Hayit Greenspan, Christos Davatzikos, James S. Duncan, Bram Van Ginneken, Anant Madabhushi, Jerry L. Prince, Daniel Rueckert, and Ronald M. Summers. 2021. A Review of Deep Learning in Medical Imaging: Imaging Traits, Technology Trends, Case Studies With Progress Highlights, and Future Promises. *Proc. IEEE* 109, 5 (2021), 820–838. <https://doi.org/10.1109/JPROC.2021.3054390>